Author/s:
Impey, RE;Lee, M;Hawkins, DA;Sutton, JM;Panjikar, S;Perugini, MA;Soares da Costa, TP

Title:
Mis-annotations of a promising antibiotic target in high-priority gram-negative pathogens

Date:
2020-05-01

Citation:
Impey, R. E., Lee, M., Hawkins, D. A., Sutton, J. M., Panjikar, S., Perugini, M. A. & Soares da Costa, T. P. (2020). Mis-annotations of a promising antibiotic target in high-priority gram-negative pathogens. FEBS Letters, 594 (9), pp.1453-1463. https://doi.org/10.1002/1873-3468.13733.

DR. MATTHIEW A. PERUGINI (Orcid ID : 0000-0001-8052-5584)

DR. TATIANA P. SOARES DA COSTA (Orcid ID : 0000-0002-6275-7485)

Received Date : 15-Nov-2019

Revised Date : 17-Dec-2019

Accepted Date : 17-Dec-2019

Article type : Communication

Mis-annotations of a Promising Antibiotic Target in High Priority Gram-Negative Pathogens

Rachael E. Impey[1], Mihwa Lee[1], Daniel A. Hawkins[1], J. Mark Sutton[2], Santosh Panjikar[3,4], Matthew A. Perugini[1,#], Tatiana P. Soares da Costa[1,#]

[1]Department of Biochemistry and Genetics, La Trobe Institute for Molecular Science, La Trobe University, Melbourne, VIC 3086, Australia.

[2]National Infection Service, Research and Development Institute, Public Health England, Porton Down, Salisbury, Wiltshire SP40JG, UK.

[3]Australian Synchrotron, ANSTO, 800 Blackburn Road, Clayton, VIC 3168, Australia.

[4]Department of Molecular Biology and Biochemistry, Monash University, Melbourne, VIC 3800, Australia.

[#]Correspondence

T. P. Soares da Costa, Department of Biochemistry and Genetics, La Trobe University, Bundoora, VIC 3086, Australia
Tel. (+61) 3 9479 2227
E-mail: T.SoaresdaCosta@latrobe.edu.au
or
M. A. Perugini, Department of Biochemistry and Genetics, La Trobe University, Bundoora, VIC 3086, Australia
Tel. (+61) 3 9479 6570
E-mail: M.Perugini@latrobe.edu.au

Running title

DHDPS mis-annotations in Gram-negative pathogens

Abbreviations

o-ABA, *o*-aminobenzaldehyde; ASA, (*S*)-aspartate semialdehyde; CD, circular dichroism; DAP, diaminopimelate; DAP-DC, diaminopimelate decarboxylase; DAP-E, diaminopimelate epimerase; DHDPR, dihydrodipicolinate reductase; DHDPS, dihydrodipicolinate synthase; HTPA, 4-hydroxy-2,3,4,5-tetrahydro-(2*S*)-dipicolinic acid; *L*-lysine, lysine; NADPH, nicotinamide adenine dinucleotide phosphate; THDP, 2,3,4,5-tetrahydropicolinate.

Keywords

antibiotic resistance, cell wall, diaminopimelate pathway, 4-hydroxy-tetrahydrodipicolinate synthase, lysine.

Conflicts of interest

The authors declare that they have no conflicts of interest with the contents of this article.

PDB ID

6UE0

ABSTRACT

The rise of antibiotic resistance combined with the lack of new products entering the market has led to bacterial infections becoming one of the biggest threats to global health. Therefore,

there is an urgent need to identify novel antibiotic targets, such as dihydrodipicolinate synthase (DHDPS), an enzyme involved in the production of essential metabolites in cell wall and protein synthesis. Here, we utilised a 7-residue sequence motif to identify mis-annotation of multiple DHDPS genes in the high-priority Gram-negative bacteria *Acinetobacter baumannii* and *Klebsiella pneumoniae*. We subsequently confirmed these mis-annotations using a combination of enzyme kinetics and X-ray crystallography. Thus, this study highlights the need to ensure genes encoding promising drug targets, like DHDPS, are annotated correctly, especially for clinically-important pathogens.

INTRODUCTION

Bacterial resistance to antibiotics is increasing, with widespread resistance no longer a threat but a reality, contributing significantly to patient morbidity and mortality [1]. Moreover, few new antibiotics are in development, with pharmaceutical companies failing to meet current clinical needs. As such, the World Health Organization (WHO) has released a priority list of bacteria that require urgent antibiotic research and development, with the top three pathogens being carbapenem-resistant *Acinetobacter baumannii*, *Pseudomonas aeruginosa* and *Enterobacteriaceae spp.* [1]. These Gram-negative bacteria cause several nosocomial infections, particularly in immunocompromised patients, including meningitis, pneumonia, bacteraemia as well as urinary tract and wound infections [1]. The range and severity of these infections highlight the importance of identifying novel drug targets against these high priority Gram-negative pathogens.

A promising target for new antibiotic development are the enzymes in the diaminopimelate (DAP) pathway that are responsible for the production of *meso*-DAP and *L*-lysine (lysine) (Fig. 1) [2–7]. In the majority of Gram-negative bacteria, *meso*-DAP is a constituent of the peptidoglycan chains within the cell wall, while lysine is essential for protein synthesis [2–9]. Importantly, the synthesis of these metabolites via the DAP pathway is unique to bacteria and plants, thus minimising potential off-target effects in humans [3,4,6,7]. The first committed step of this pathway is the condensation of pyruvate and (*S*)-aspartate semialdehyde (ASA) to

produce 4-hydroxy-2,3,4,5-tetrahydro-(2*S*)-dipicolinic acid (HTPA) catalysed by the class I aldolase 4-hydroxy-tetrahydrodipicolinate synthase (**EC 4.3.3.7**), commonly referred to as dihydrodipicolinate synthase (DHDPS) (Fig. 1) [2,10]. HTPA is subsequently reduced to 2,3,4,5-tetrahydropicolinate (THDP) using the NAD(P)H-dependent enzyme 4-hydroxy-tetrahydrodipicolinate reductase (**EC 1.17.1.8**), herein referred to as dihydrodipicolinate reductase (DHDPR) (Fig. 1) [6,11,12]. At this point, the DAP pathway diverges into one of four sub-pathways, with each resulting in the production of *meso*-DAP (Fig. 1) [6,7,10]. The sub-pathways are organism-dependent [6,7,10] with, for example, Gram-negative bacteria utilising the succinyl sub-pathway that yields *LL*-DAP before conversion to *meso*-DAP by diaminopimelate epimerase (DAP-E, **EC 5.1.1.7**) (Fig. 1) [4,6]. Finally, *meso*-DAP is used either directly in the crosslinking of the peptidoglycan layer in Gram-negative bacteria, or decarboxylated to lysine by diaminopimelate decarboxylase (DAP-DC, **EC 4.1.1.20**) (Fig. 1) [4,13,14]. The production of lysine in this final step also serves as a negative feedback loop, where lysine can bind and allosterically inhibit the DHDPS enzyme [15–17].

Given DHDPS is involved in the first committed and rate limiting step of the DAP pathway, several studies have focused on demonstrating the essentiality of its encoding gene, *dapA*, for bacterial survival [18–22]. Typically, bacteria contain a single *dapA* gene. However, we have recently identified that *P. aeruginosa* has up to 4 annotated *dapA* genes, of which only two encode functional DHDPS enzymes [23]. Mis-annotated *dapA* genes have also been previously observed in *Agrobacterium tumefaciens*, with 9 out of the 10 annotated *dapA* genes yielding enzymes that lacked DHDPS activity [24]. Another recent study showed that fungi do not contain an active DHDPS gene despite being annotated in various sequence and structure databases [25]. Indeed, this study postulated a 7-residue motif ($TTX_{(57-61)}YYX_{(22-26)}YX_{(3-5)}RX_{(18-22)}K$, where X represents the length, shown by the numbers in brackets, of the undefined amino acid sequences separating the signature residues) to identify functional DHDPS sequences [25]. Without accurate and reliable similarity-based assignments, the amount of mis-annotation errors in genomes could account for up to 30% of annotated protein functions [26]. There is also conjecture about using descriptions of genes as "putative" or "like", as currently there are no defined parameters for this classification [27]. The use of these terms further enhances the potential for mis-annotations [27].

In this study, we have identified that *A. baumannii* and *K. pneumoniae* have been suggested to contain multiple *dapA* genes. We then set out to characterise the gene products from these priority Gram-negative pathogens using a combination of sequence analysis, circular

dichroism spectroscopy, enzyme kinetics and X-ray crystallography. Importantly, this work supports recent studies that have used a combination of sequence and structure/function workflows to reliably identify the annotated *dapA* genes that encode functional DHDPS enzymes [24,25]. Such strategies are critical to ensure correct gene annotations are based on key signature motifs that are validated experimentally.

RESULTS

Annotated dapA genes

The annotated *dapA* genes in *K. pneumoniae* (Kp) were identified using the NCBI database. The search yielded four putative genes, with Kp*dapA1* (**GENBANK ID: CCN30951.1**), Kp*dapA2* (**GENBANK ID: WP_107318840.1**) and Kp*dapA4* (**GENBANK ID: CCN29687.1**) found in the genome of the reference strain Ecl8 (**GENBANK ID: GCA_000315385.1**), whilst Kp*dapA3* (**GENBANK ID: KGJ39907.1**) was identified in the CDH3823 genome (**GENBANK ID: JQDX00000000**). To further investigate the putative function of these genes, we performed an alignment with their translated protein sequences compared to *E. coli* (Ec) DHDPS (Fig. 2). KpDapA1 was shown to possess the highest sequence identity (87.6%) to EcDHDPS. The sequence alignment also shows low similarity between the KpDapA proteins, with KpDapA1 and KpDapA4 displaying the highest identity to one another (29.5%). Interestingly, KpDapA3 has a high degree of similarity to the mis-annotated *P. aeruginosa* (Pa) DapA3 protein (**UNIPROT ID: Q9I490**) (data not shown), which encodes a 1-pyrroline-4-hydrozy-2-carboxylate (Pyr4H2C) deaminase enzyme [23]. Nevertheless, based on our previous findings [23–25], sequence similarity alone is an unreliable determinant of DHDPS function. Therefore, we examined whether these sequences contained a 7-residue signature sequence motif that has been proposed to be essential in *bona fide* DHDPS enzymes [25]. KpDapA1 was found to be the only protein with all 7 active site residues that are critical for DHDPS catalysis, while both KpDapA2 and KpDapA4 have 4 of the 7 residues and KpDapA3 contains only 2 of the 7 (Fig. 2).

Similar to *K. pneumoniae*, our investigation revealed that *Acinetobacter baumannii* (Ab) had four annotated *dapA* genes; Ab*dapA1* (**GENBANK ID: KMV04290.1**), Ab*dapA2* (**GENBANK ID: KRJ74652.1),** Ab*dapA3* (**GENBANK ID: KMV01952.1**) and Ab*dapA4* (**GENBANK ID: AZK38617.1**). The crystal structure of AbDapA1 has been deposited (**PDB ID: 3TAK**), although there is no accompanying functional data. Comparison of all four gene products revealed that the sequence with the highest similarity to EcDHDPS was

that of the gene product of Ab*dapA1*, displaying ~50% identity. Furthermore, we confirmed that only this protein contains the 7-residue DHDPS functional signature motif (Fig. 2). We therefore hypothesise that Kp*dapA1* and Ab*dapA1* encode functional DHDPS enzymes. We set out to confirm this by characterising the corresponding recombinant proteins.

Validation of DHDPS activity

To experimentally validate the 7-residue motif, recombinant KpDapA1-4 proteins were overexpressed in *E. coli* and purified to >90% homogeneity (Fig. 3A). Circular dichroism (CD) spectroscopy showed a single maximum at ~195 nm and a broad minimum spanning ~205-225 nm. This confirms that the recombinant proteins were folded to form a mixed α/β secondary structure (Fig. 3B), which is known for aldolase or TIM-barrel enzymes, such as DHDPS [28,29]. Next, the qualitative *o*-aminobenzaldehyde (*o*-ABA) assay was used to assess DHDPS enzymatic activity *in vitro*. Activity is indicated by the production of a purple chromophore, with no discernible colour change indicative of no DHDPS activity [30,31]. A purple colour change was only observed for KpDapA1, which was similar to the positive control (Fig. 3C). This confirms our hypothesis that Kp*dapA1* encodes the only functional DHDPS from *K. pneumoniae*. This protein will be referred to from herein as KpDHDPS.

Given that the 7-residue signature prediction was validated experimentally in *K. pneumoniae*, the predicted functional DHDPS enzyme from *A. baumannii*, AbDapA1, was subsequently overexpressed in *E. coli* and purified to >90% homogeneity (Fig. 4A). CD spectroscopy again confirmed a mixed α/β secondary structure (Fig. 4B), consistent with the previously solved structure (**PDB ID: 3TAK**); whilst the *o*-ABA assay was used to qualitatively ascertain the production of DHDPS enzymatic activity (Fig. 4C). This confirms that Ab*dapA1* codes for a functional DHDPS enzyme, hereafter referred to as AbDHDPS.

DHDPS functional characterisation

To further characterise the confirmed DHDPS enzymes, their kinetic parameters were quantified using the DHDPS-DHDPR coupled assay [12,32]. Initial rate was monitored by varying the concentrations of both substrates, pyruvate and ASA, and data were globally fitted to a bi-substrate ping-pong model without substrate inhibition (Fig. 5) [33]. For KpDHDPS, the resulting K_M values for pyruvate and ASA were calculated to be 1.2 mM and 0.34 mM, respectively, with a turnover number (k_{cat}) of 290 s^{-1}. These yielded catalytic

efficiency (k_{cat}/K_M) values of 2.4 × 10^5 $s^{-1}{\cdot}M^{-1}$ and 1.9 × 10^6 $s^{-1}{\cdot}M^{-1}$ for pyruvate and ASA, respectively, which are consistent with previously characterised bacterial DHDPS enzymes [24,34]. Kinetic characterisation of AbDHDPS yielded a K_M value for pyruvate of 0.25 mM, and 0.036 mM for ASA, resulting in a k_{cat} of 48 s^{-1} (Fig. 5). Calculated catalytic efficiency values of 1.9 × 10^5 $s^{-1}{\cdot}M^{-1}$ and 1.3 × 10^6 $s^{-1}{\cdot}M^{-1}$ for pyruvate and ASA, respectively, were determined, which are consistent with what we observe for KpDHDPS and previously reported values for other bacterial DHDPS orthologues [23,35]. To determine the allosteric inhibition of these enzymes, increasing concentrations of lysine were titrated in the DHDPS-DHDPR coupled assay. The resulting IC_{50} value for both KpDHDPS and AbDHDPS was 160 μM (Table 1). This is consistent with previously reported bacterial DHDPS enzymes, including EcDHDPS and PaDHDPS2 (Table 1) [23,35].

Implications for inhibitor design

Although some DHDPS enzymes are not inhibited by lysine, the high degree of conservation at the active site across bacterial species allows for the potential identification of broad-spectrum inhibitors [36]. To illustrate this, KpDHDPS was crystallised in the presence of the substrate pyruvate, and the structure was solved using molecular replacement and refined to 1.89 Å resolution (Tables 2 and 3). The overall quaternary structure of KpDHDPS is consistent with previously characterised bacterial DHDPS enzymes, including orthologues from *E. coli* (**PDB ID: 3DU0**, root-mean-square-deviation (r.m.s.d.) of 0.50 Å for 584 Cα atoms) and *A. baumannii* (**PDB ID: 3TAK**, r.m.s.d. of 1.19 Å for 582 Cα atoms), with a head-to-head dimer-of-dimers arrangement to form the tetramer (Fig. 6A). The active site is located at the C-terminal end of the α/β TIM-barrel, with tyrosine 107 (*E. coli* numbering) interdigitating between the two monomers across the dimerisation interface, forming the complete catalytic triad required for enzymatic activity [37]. The pyruvate molecule was found to form a Schiff base with lysine 161 (*E. coli* numbering) in the active site, which is consistent with other pyruvate-bound DHDPS enzymes [37].

We first superposed the active site of KpDHDPS with the structures of the now validated AbDHDPS (**PDB ID: 3TAK**) and EcDHDPS (**PDB ID: 3DU0**) in pyruvate-bound forms, and the apo PaDHDPS2 structure (**PDB: 3NOE**). As shown in Figure 6B, the active site residues in these high priority Gram-negative pathogens are 100% conserved, representing a possible 'druggable' site for novel broad-spectrum antibiotic development. Subsequently, we

superposed the structure of EcDHDPS (**PDB ID: 3DU0**) with that of the mis-annotated PaDapA4 enzyme (**PDB ID: 3NA8**), which has previously been shown not to possess DHDPS activity and only contains 4 of the 7 key DHDPS residues [23]. Not surprisingly, we observe a low level of conservation in the active site with differences at positions 45, 106 and 138 (*E. coli* numbering) (Fig. 6C). Most notably, tyrosine 106 is replaced by a serine, which in turn changes the position of the interdigitating tyrosine 107 from the adjacent monomer (*E. coli* numbering) (Fig. 6C). These differences significantly alter the conformation of the active site, highlighting the need for correct annotations and validation of the activity of promising drug targets.

DISCUSSION

The development of whole genome sequencing in the late 1990s led to a boom in gene annotations based often on limited homology [38]. Sequencing is now relatively routine and typically involves automatic computerised annotations. However, this method relies on the assumption that sequence similarity equates to a similar function [39]. This has resulted in an astounding number of gene mis-annotations across multiple species. One striking example is the annotation of *Haemophilus influenzae*, which had over 148 amendments within just 4 weeks of publication [40]. More recently, a study highlighted that one out of eight genes in the human genome are annotated differently among different database sets [41]. Statistical analysis of genome annotations have estimated the error rate to even be as high as 49% [42]. This is exemplified with the investigation of carbohydrate-active enzyme genes in *Fibrobacter succinogenes*, in which out of the 20 novel genes discovered, 12 were annotated to functions unrelated to the observed enzymatic activity [43]. These mis-annotations can lead to what is described as "the snowball effect" [44]. Simply, when a single gene is mis-annotated, a multitude of similar genes are then subsequently mis-annotated based on the first [44].

Here, we describe the repeated mis-annotation of the DHDPS-encoding *dapA* gene in two clinically important Gram-negative pathogens, *A. baumannii* and *K. pneumoniae*. Specifically, we used a recently reported 7-residue signature motif [25] to predict DHDPS activity for the *dapA*-gene encoding products in *A. baumannii* and *K. pneumoniae*, followed by experimental validations *in vitro*. In summary, despite sequence databases suggesting *A. baumannii* and *K. pneumoniae* contain 4 *dapA* genes, we show that these pathogens only possess a single gene encoding a functional DHDPS enzyme. Importantly, we determined the

crystal structure of the *bona fide* DHDPS enzyme from *K. pneumoniae* DHDPS, which formed a tetrameric structure consistent with other bacterial DHDPS enzymes. Indeed, comparison to the structures of the validated DHDPS enzymes from *A. baumannii, P. aeruginosa* and *E. coli* reveal a high degree of conservation, especially within the active site. We then further compared the active site of the *E. coli* DHDPS enzyme to the mis-annotated *P. aeruginosa* DapA4, illustrating a lesser degree of conservation as expected given the lack of DHDPS activity observed with this enzyme. Thus, this study highlights the need to validate the enzymatic activity of annotated drug targets, like DHDPS, and provides an important platform for the rational design of broad-spectrum DHDPS inhibitors as an emerging class of antibiotics for the treatment of infections caused by these high priority Gram-negative pathogens.

METHODS

Sequence Analysis

Three putative *dapA* genes were identified in the *K. pneumoniae* genome Ecl8, with a further *dapA* gene found in the CDH3823 genome [45]. All four putative *dapA* genes for *A. baumannii* were identified in the AB030 genome [46]. Sequence alignments with *E. coli* DHDPS (**UNIPROT ID: P0A6L2**) were performed using the ClustalW algorithm [47] incorporated in BIOEDIT (v.7.2.0) [48]. All alignments used *E. coli* residue numbering.

Protein Expression and Purification

The synthetic genes coding for *K. pneumoniae* and *A. baumannii* proteins with a hexa-histidine tag were codon optimised, synthesised and ligated into a pET28a expression vector by Bioneer Pacific (Bioneer Pacific, Kew East, Victoria, Australia). Recombinant proteins were expressed in *E. coli* BL21 (DE3) cells and purified using immobilised metal affinity chromatography (IMAC) as previously described [49]. Briefly, recombinant proteins were expressed upon addition of 0.5 mM isopropyl β-D-1-thiogalactopyranoside (IPTG) in Luria-Bertani (LB) broth at 16 °C for 18 hr for *K. pneumoniae* and *A. baumannii* proteins or 37 °C for 4 hr for *E. coli* proteins. Cells were harvested via centrifugation at 5000 × g at 4 °C and sonicated in 20 mM Tris, 150 mM NaCl, 20 mM imidazole, pH 8.0 using a Vibra Cell VC40 (Sonics and Material, Newtown, Connecticut, USA). Recombinant His-tagged proteins were purified using a 5 ml IMAC column (Bio-Rad Laboratories, Gladesville, New South Wales, Australia) and stored in 20 mM Tris, 150 mM NaCl, pH 8.0.

Circular Dichroism (CD) Spectroscopy

CD spectroscopy was performed as previously described [12,50] in an Aviv Model 420 CD spectrometer. Protein samples were prepared at 150-200 μg·ml^{-1} in 20 mM NaH_2PO_4, 50 mM KF, pH 8.0. Spectra were obtained between 190 and 250 nm in 1 nm increments with 5 s averaging time at a temperature of 20 °C using 1 mm quartz cuvettes. Analysis was performed employing CDPro, and the data was fitted using the CONTINLL database with the SP22X reference set [51,52].

o-Aminobenzaldehyde Assay

To qualitatively assess for DHDPS activity, the colorimetric *o*-aminobenzaldehyde (*o*-ABA) assay was employed as previously described [17,30,31]. Assays were performed in a 96-well plate with reactions initiated with the addition of 5 μl of 0.5 mg·ml^{-1} protein sample to 100 μl of mastermix. Reactions were terminated after 30 min with 10 μl of 10% (v/v) trichloroacetic acid. Recombinant *E. coli* DHDPS and *E. coli* DHDPR were used as a positive and negative controls, respectively. DHDPS activity was confirmed by the production of a purple chromophore.

Coupled Assay

The DHDPS-DHDPR coupled assay was used to quantify DHDPS activity as previously described [32,53,54]. Briefly, the substrate turnover was measured via the associated oxidation of NADPH at $Abs_{340\ nm}$ ($\varepsilon_{340\ nm}$ = 6220 M^{-1} cm^{-1}) in a Cary 4000 UV/Vis spectrophotometer (Varian, Mulgrave, Victoria, Australia). All assays were performed in triplicate (n = 3) and incubated at 37 °C for 12 min before initiating the reaction by the addition of ASA. For the determination of the Michaelis-Menten constants (K_M), pyruvate and ASA were varied simultaneously ranging from 0.125 – 4 mM and 0.05 – 1 mM, respectively, with KpDHDPS kept constant at 5 μg·ml^{-1} and AbDHDPS at 3 μg·ml^{-1}. Initial velocity data were analysed employing ENZFITTER v.2.0.18 (Biosoft, Cambridge, UK) and fitted to the ping-pong mechanism using Equation 1.

Equation 1:

$$v=(V_{max}*A*B)/(K_{M,A}*B + K_{M,B}*A + A*B)$$

Where v = initial velocity, V_{max} = limiting maximal velocity, A = [pyruvate], B = [ASA], $K_{M,A}$ = limiting Michaelis-Menten constant for A, $K_{M,B}$ = limiting Michaelis-Menten constant for B.

Lysine inhibition was measured by titrating concentrations of lysine ranging from 0.078 – 1 mM against KpDHDPS and AbDHDPS. Initial velocity data were analysed using GraphPad Prism v.8.2 (GraphPad, San Diego, California, USA) and fitted to the log(inhibitor) vs response (variable slope) using Equation 2.

Equation 2:

$$Y = Bottom + (Top-Bottom) / (1+10^{((Log IC_{50}-X)*HillSlope)})$$

Where X = log of lysine concentration, Y = response, Top and Bottom = plateaus in the same units as Y, Hill slope = slope factor.

Crystallisation and X-ray Diffraction Data Collection

KpDHDPS was crystallised using the hanging-drop vapour diffusion method at 20 °C. Diffraction-quality crystals grew after 2 days in drops consisting of equal volume (2 µl) of KpDHDPS (10 mg·ml^{-1} in 20 mM Tris, 150 mM NaCl, pH 8.0) and reservoir solution (100 mM Tris pH 7.5, 2 M ammonium sulfate, 5 mM pyruvate) equilibrated against 1 ml of reservoir solution. X-ray diffraction was performed at the microfocus beamline (MX2) of the Australian Synchrotron [55]. The crystals were flash-cooled in liquid nitrogen and transferred to a stream of nitrogen gas at 100 K at the goniometer. 180° of the diffraction data were collected at a wavelength of 0.9537 Å using an EIGER-16M detector with 0.1° oscillation and 0.1 sec exposure of 0% attenuated beam per frame. The data were indexed and integrated with XDS [56] and scaled using AIMLESS [57]. The data were processed in space group $P2_12_12$, with unit-cell parameters a = 105.6, b = 114.2, c = 55.3 Å. The asymmetric unit is estimated to contain two monomers, with a corresponding crystal volume per protein weight of 2.67 Å^3 Da^{-1} and a solvent content of 54.0%. Data collection and processing statistics are detailed in Table 2.

Structure Solution and Refinement

Molecular replacement was performed using PHASER [58] within the CCP4 suite [59]. Chain A of the EcDHDPS structure (**PDB ID: 1YXC**) was used as a search model after removing all non-protein atoms. CHAINSAW was used to replace all non-identical residues

with alanine [60]. Two monomers were found in the asymmetric unit with a log-likelihood gain of 59712 and a *Z*-score of 72.7. Iterative model building with COOT [61] and refinement using REFMAC [62] were performed. The quality of the model was validated using MOLPROBITY [63]. The refinement statistics are included in Table 3. The atomic co-ordinates and experimental structure factors were deposited in the Protein Data Bank under accession code 6UE0.

AUTHOR CONTRIBUTIONS

T.P.S.C., M.A.P. and R.E.I. planned the experiments; R.E.I. and D.A.H. performed the experiments; R.E.I., T.P.S.C., M.A.P., M.L., S.P. and J.M.S. analysed the data; R.E.I., M.A.P. and T.P.S.C. wrote the paper.

ACKNOWLEDGEMENTS

T.P.S.C. would like to thank the National Health and Medical Research Council of Australia (APP1091976) and Australian Research Council (DE190100806) for fellowship and funding support, and M.A.P. and S.P. the Australian Research Council for funding support (DP150103313). R.E.I. is supported by an Australian Research Training scholarship and acknowledges the British Society for Antimicrobial Chemotherapy for funding support. M.L. is supported by the Tracey Banivanua Mar fellowship from La Trobe University. We thank Dr. Janni Christensen for the insurgent technical support. We acknowledge the use of the MX2 beamline at the Australian Synchrotron and the CSIRO Collaborative Crystallisation Centre (www.csiro/C3; Melbourne, Australia). We also thank the La Trobe University Comprehensive Proteomics Platform for providing infrastructure support.

REFERENCES

1. Tacconelli E, Carrara E, Savoldi A, Harbarth S, Mendelson M, Monnet DL, Pulcini C, Kahlmeter G, Kluytmans J, Carmeli Y, Ouellette M, Outterson K, Patel J, Cavaleri M, Cox EM, Houchens CR, Grayson ML, Hansen P, Singh N, Theuretzbacher U, Magrini N, Aboderin AO, Al-Abri SS, Awang Jalil N, Benzonana N, Bhattacharya S, Brink AJ, Burkert FR, Cars O, Cornaglia G, Dyar OJ, Friedrich AW, Gales AC, Gandra S, Giske CG, Goff DA, Goossens H, Gottlieb T, Guzman Blanco M,

Hryniewicz W, Kattula D, Jinks T, Kanj SS, Kerr L, Kieny M-P, Kim YS, Kozlov RS, Labarca J, Laxminarayan R, Leder K, Leibovici L, Levy-Hara G, Littman J, Malhotra-Kumar S, Manchanda V, Moja L, Ndoye B, Pan A, Paterson DL, Paul M, Qiu H, Ramon-Pardo P, Rodríguez-Baño J, Sanguinetti M, Sengupta S, Sharland M, Si-Mehand M, Silver LL, Song W, Steinbakk M, Thomsen J, Thwaites GE, van der Meer JW, Van Kinh N, Vega S, Villegas MV, Wechsler-Fördös A, Wertheim HFL, Wesangula E, Woodford N, Yilmaz FO & Zorzet A (2018) Discovery, research, and development of new antibiotics: the WHO priority list of antibiotic-resistant bacteria and tuberculosis. *Lancet Infect Dis* 18, 318–327.

2. Soares da Costa TP, Abbott BM, Gendall AR, Panjikar S & Perugini MA (2017) Molecular evolution of an oligomeric biocatalyst functioning in lysine biosynthesis. *Biophys Rev* 4, 153–162.
3. Impey RE & Soares da Costa T Review: Targeting the biosynthesis and incorporation of amino acids into peptidoglycan as an antibiotic approach against Gram negative bacteria. *EC Microbiol*, 10.
4. Hutton CA, Perugini MA & Gerrard JA (2007) Inhibition of lysine biosynthesis: an evolving antibiotic strategy. *Mol Biosyst* 3, 458–465.
5. Hermann M, Thevenet NJ, Coudert-Maratier MM & Vandecasteele J-P (1972) Consequences of lysine oversynthesis in Pseudomonas mutants insensitive to feedback inhibition. *Eur J Biochem* 30, 100–106.
6. Dogovski C, Atkinson SC, Dommaraju SR, Downton M, Hor L, Moore S, Paxman JJ, Peverelli MG, Qiu TW & Reumann M (2012) Enzymology of bacterial lysine biosynthesis. In *Biochemistry (D Ekinci, ed.)* InTech Open Access Publisher, London, UK.
7. Dogovski C, Atkinson SC, Dommaraju SR, Hor L, Dobson RCJ, Hutton CA, Gerrard JA & Perugini MA (2009) Lysine biosynthesis in bacteria: an unchartered pathway for novel antibiotic design. In *Encyclopedia Of Life Support Systems (H Doell, ed.)* pp. 116–136. EOLSS Publishers, Paris, France.
8. Vollmer W & Seligman SJ (2010) Architecture of peptidoglycan: more data and more models. *Trends Microbiol* 18, 59–66.
9. Royet J & Dziarski R (2007) Peptidoglycan recognition proteins: pleiotropic sensors and effectors of antimicrobial defences. *Nat Rev Microbiol* 5, 264–277.
10. Hall C & Soares da Costa TP (2018) Lysine: biosynthesis, catabolism and roles. *WikiJ Sci* 1, 4.

11. Devenish SRA, Blunt JW & Gerrard JA (2010) NMR studies uncover alternate substrates for dihydrodipicolinate synthase and suggest that dihydrodipicolinate reductase is also a dehydratase. *J Med Chem* 53, 4808–4812.

12. Christensen JB, Soares da Costa TP, Faou P, Pearce FG, Panjikar S & Perugini MA (2016) Structure and function of cyanobacterial DHDPS and DHDPR. *Sci Rep* 6, 37111.

13. Peverelli MG, Costa TPS da, Kirby N & Perugini MA (2016) Dimerization of bacterial diaminopimelate decarboxylase is essential for catalysis. *J Biol Chem* 291, 9785–9795.

14. Ray SS, Bonanno JB, Rajashankar KR, Pinho MG, He G, De Lencastre H, Tomasz A & Burley SK (2002) Cocrystal structures of diaminopimelate decarboxylase: mechanism, evolution, and inhibition of an antibiotic resistance accessory factor. *Structure* 10, 1499–1508.

15. Karsten WE (1997) Dihydrodipicolinate synthase from *Escherichia coli*: pH dependent changes in the kinetic mechanism and kinetic mechanism of allosteric inhibition by *L*-lysine. *Biochemistry* 36, 1730–1739.

16. Dobson RCJ, Griffin MDW, Jameson GB & Gerrard JA (2005) The crystal structures of native and (*S*)-lysine-bound dihydrodipicolinate synthase from *Escherichia coli* with improved resolution show new features of biological significance. *Acta Crystallogr* 61, 1116–1124.

17. Soares da Costa TP, Desbois S, Dogovski C, Gorman MA, Ketaren NE, Paxman JJ, Siddiqui T, Zammit LM, Abbott BM, Robins-Browne RM, Parker MW, Jameson GB, Hall NE, Panjikar S & Perugini MA (2016) Structural determinants defining the allosteric inhibition of an essential antibiotic target. *Structure* 24, 1282–1291.

18. Dogovski C, Gorman MA, Ketaren NE, Praszkier J, Zammit LM, Mertens HD, Bryant G, Yang J, Griffin MDW, Pearce FG, Gerrard JA, Jameson GB, Parker MW, Robins-Browne RM & Perugini MA (2013) From knock-out phenotype to three-dimensional structure of a promising antibiotic target from *Streptococcus pneumoniae*. *PLOS ONE* 8, e83419.

19. Gerdes SY, Scholle MD, Campbell JW, Balázsi G, Ravasz E, Daugherty MD, Somera AL, Kyrpides NC, Anderson I, Gelfand MS, Bhattacharya A, Kapatral V, D'Souza M, Baev MV, Grechkin Y, Mseeh F, Fonstein MY, Overbeek R, Barabási A-L, Oltvai ZN & Osterman AL (2003) Experimental determination and system level analysis of essential genes in *Escherichia coli* MG1655. *J Bacteriol* 185, 5673–5684.

20. Bukhari AI & Taylor AL (1971) Genetic analysis of diaminopimelic acid- and lysine-requiring mutants of *Escherichia coli*. *J Bacteriol* 105, 844–854.
21. Kobayashi K, Ehrlich SD, Albertini A, Amati G, Andersen KK, Arnaud M, Asai K, Ashikaga S, Aymerich S, Bessieres P, Boland F, Brignell SC, Bron S, Bunai K, Chapuis J, Christiansen LC, Danchin A, Débarbouille M, Dervyn E, Deuerling E, Devine K, Devine SK, Dreesen O, Errington J, Fillinger S, Foster SJ, Fujita Y, Galizzi A, Gardan R, Eschevins C, Fukushima T, Haga K, Harwood CR, Hecker M, Hosoya D, Hullo MF, Kakeshita H, Karamata D, Kasahara Y, Kawamura F, Koga K, Koski P, Kuwana R, Imamura D, Ishimaru M, Ishikawa S, Ishio I, Le Coq D, Masson A, Mauël C, Meima R, Mellado RP, Moir A, Moriya S, Nagakawa E, Nanamiya H, Nakai S, Nygaard P, Ogura M, Ohanan T, O'Reilly M, O'Rourke M, Pragai Z, Pooley HM, Rapoport G, Rawlins JP, Rivas LA, Rivolta C, Sadaie A, Sadaie Y, Sarvas M, Sato T, Saxild HH, Scanlan E, Schumann W, Seegers JFML, Sekiguchi J, Sekowska A, Séror SJ, Simon M, Stragier P, Studer R, Takamatsu H, Tanaka T, Takeuchi M, Thomaides HB, Vagner V, van Dijl JM, Watabe K, Wipat A, Yamamoto H, Yamamoto M, Yamamoto Y, Yamane K, Yata K, Yoshida K, Yoshikawa H, Zuber U & Ogasawara N (2003) Essential *Bacillus subtilis* genes. *Proc Natl Acad Sci* 100, 4678–4683.
22. Becker D, Selbach M, Rollenhagen C, Ballmaier M, Meyer TF, Mann M & Bumann D (2006) Robust Salmonella metabolism limits possibilities for new antimicrobials. *Nature* 440, 303–307.
23. Impey RE, Panjikar S, Hall CJ, Bock LJ, Sutton JM, Perugini MA & Soares da Costa TP (2019) Identification of two dihydrodipicolinate synthase isoforms from *Pseudomonas aeruginosa* that differ in allosteric regulation. *FEBS J*.
24. Atkinson SC, Hor L, Dogovski C, Dobson RCJ & Perugini MA (2014) Identification of the *bona fide* DHDPS from a common plant pathogen. *Proteins* 82, 1869–1883.
25. Desbois S, John UP & Perugini MA (2018) Dihydrodipicolinate synthase is absent in fungi. *Biochimie* 152, 73–84.
26. Devos D & Valencia A (2001) Intrinsic errors in genome annotation. *Trends Genet* 17, 429–431.
27. Schnoes AM, Brown SD, Dodevski I & Babbitt PC (2009) Annotation error in public databases: misannotation of molecular function in enzyme superfamilies. *PLOS Comp Biol* 5, e1000605.

28. Dobson RCJ, Griffin MDW, Roberts SJ & Gerrard JA (2004) Dihydrodipicolinate synthase (DHDPS) from *Escherichia coli* displays partial mixed inhibition with respect to its first substrate, pyruvate. *Biochimie* 86, 311–315.

29. Burgess BR, Dobson RCJ, Bailey MF, Atkinson SC, Griffin MDW, Jameson GB, Parker MW, Gerrard JA & Perugini MA (2008) Structure and evolution of a novel dimeric enzyme from a clinically important bacterial pathogen. *J Biol Chem* 283, 27598–27603.

30. Mitsakos V, Devenish SRA, O'Donnell PA, Gerrard JA & Hutton CA (2011) LC–MS and NMR characterization of the purple chromophore formed in the *o*-aminobenzaldehyde assay of dihydrodipicolinate synthase. *Bioorg Med Chem* 19, 1535–1540.

31. Yugari Y & Gilvarg C (1965) The condensation step in diaminopimelate synthesis. *J Biol Chem* 240, 4710–4716.

32. Coulter CV, Gerrard JA, Kraunsoe JAE & Pratt AJ (1999) *Escherichia coli* dihydrodipicolinate synthase and dihydrodipicolinate reductase: kinetic and inhibition studies of two putative herbicide targets. *J Pest Sci* 55, 887–895.

33. Muscroft-Taylor AC, Soares da Costa TP & Gerrard JA (2010) New insights into the mechanism of dihydrodipicolinate synthase using isothermal titration calorimetry. *Biochimie* 92, 254–262.

34. Voss JE, Scally SW, Taylor NL, Atkinson SC, Griffin MDW, Hutton CA, Parker MW, Alderton MR, Gerrard JA, Dobson RCJ, Dogovski C & Perugini MA (2010) Substrate-mediated stabilization of a tetrameric drug target reveals Achilles heel in anthrax. *J Biol Chem* 285, 5188–5195.

35. Soares da Costa TP, Muscroft-Taylor AC, Dobson RCJ, Devenish SRA, Jameson GB & Gerrard JA (2010) How essential is the 'essential' active-site lysine in dihydrodipicolinate synthase? *Biochimie* 92, 837–845.

36. Christoff RM, Gardhi CK, Soares da Costa TP, Perugini MA & Abbott BM (2019) Pursuing DHDPS: an enzyme of unrealised potential as a novel antibacterial target. *MedChemComm* 10, 1581–1588.

37. Dobson RCJ, Valegård K & Gerrard JA (2004) The crystal structure of three site-directed mutants of *Escherichia coli* dihydrodipicolinate synthase: further evidence for a catalytic triad. *J Mol Biol* 338, 329–339.

38. Nobre T, Campos MD, Lucic-Mercy E & Arnholdt-Schmitt B (2016) Misannotation Awareness: A Tale of Two Gene-Groups. *Front. Plant Sci.* 7.

39. Gilks WR, Audit B, De Angelis D, Tsoka S & Ouzounis CA (2002) Modeling the percolation of annotation errors in a database of protein sequences. *Bioinformatics* 18, 1641–1649.

40. Casari G, Andrade MA, Bork P, Boyle J, Daruvar A, Ouzounis C, Schneider R, Tamames J, Valencia A & Sander C (1995) Challenging times for bioinformatics. *Nature* 376, 647–648.

41. Abascal F, Juan D, Jungreis I, Martinez L, Rigau M, Rodriguez JM, Vazquez J & Tress ML (2018) Loose ends: almost one in five human genes still have unresolved coding status. *Nucleic Acids Res* 46, 7070–7084.

42. Jones CE, Brown AL & Baumann U (2007) Estimating the annotation error rate of curated GO database sequence annotations. *BMC Bioinformatics* 8, 170.

43. Brumm P, Mead D, Boyum J, Drinkwater C, Gowda K, Stevenson D & Weimer P (2011) Functional annotation of *Fibrobacter succinogenes* S85 carbohydrate active enzymes. *Appl Biochem Biotechnol* 163, 649–657.

44. Jabbari K, Cruveiller S, Clay O, Le Saux J & Bernardi G (2004) The new genes of rice: a closer look. *Trends Plant Sci* 9, 281–285.

45. Greninger AL, Chorny I, Knowles S, Ng VL & Chaturvedi V (2015) Draft genome sequences of four NDM-1-producing *Klebsiella pneumoniae* strains from a health care facility in Northern California. *Genome Announc* 3.

46. Loewen PC, Alsaadi Y, Fernando D & Kumar A (2014) Genome sequence of an extremely drug-resistant clinical isolate of *Acinetobacter baumannii* strain AB030. *Genome Announc* 2.

47. Thompson JD, Higgins DG & Gibson TJ (1994) CLUSTAL W: improving the sensitivity of progressive multiple sequence alignment through sequence weighting, position-specific gap penalties and weight matrix choice. *Nucleic Acids Res.* 22, 4673–4680.

48. Hall T (2011) BioEdit: An important software for molecular biology. *GERF Bull BioSci* 2, 60–61.

49. Gupta R, Soares da Costa TP, Faou P, Dogovski C & Perugini MA (2018) Comparison of untagged and his-tagged dihydrodipicolinate synthase from the enteric pathogen *Vibrio cholerae*. *Protein Expr Purif* 145, 85–93.

50. Atkinson SC, Dogovski C, Downton MT, Czabotar PE, Dobson RCJ, Gerrard JA, Wagner J & Perugini MA (2013) Structural, kinetic and computational investigation of *Vitis vinifera* DHDPS reveals new insight into the mechanism of lysine-mediated allosteric inhibition. *Plant Mol Biol* 81, 431–446.

51. Sreerama N & Woody RW (2000) Estimation of protein secondary structure from circular dichroism spectra: comparison of CONTIN, SELCON, and CDSSTR methods with an expanded reference set. *Anal Biochem* 287, 252–260.

52. Johnson WC (1999) Analyzing protein circular dichroism spectra for accurate secondary structures. *Proteins* 35, 307–312.

53. Pearce FG, Perugini MA, Mckerchar HJ & Gerrard JA (2006) Dihydrodipicolinate synthase from *Thermotoga maritima*. *Biochem J* 400, 359–366.

54. Dobson RCJ, Devenish SRA, Turner LA, Clifford VR, Pearce FG, Jameson GB & Gerrard JA (2005) Role of arginine 138 in the catalysis and regulation of *Escherichia coli* dihydrodipicolinate synthase. *Biochemistry* 44, 13007–13013.

55. Aragão D, Aishima J, Cherukuvada H, Clarken R, Clift M, Cowieson NP, Ericsson DJ, Gee CL, Macedo S, Mudie N, Panjikar S, Price JR, Riboldi-Tunnicliffe A, Rostan R, Williamson R & Caradoc-Davies TT (2018) MX2: a high-flux undulator microfocus beamline serving both the chemical and macromolecular crystallography communities at the Australian Synchrotron. *J Synchrotron Radiat* 25, 885–891.

56. Kabsch W (2010) XDS. *Acta Crystallogr D Biol Crystallogr* 66, 125–132.

57. Evans PR & Murshudov GN (2013) How good are my data and what is the resolution? *Acta Crystallogr D Biol Crystallogr* 69, 1204–1214.

58. McCoy AJ, Grosse-Kunstleve RW, Adams PD, Winn MD, Storoni LC & Read RJ (2007) Phaser crystallographic software. *J Appl Cryst* 40, 658–674.

59. Winn MD, Ballard CC, Cowtan KD, Dodson EJ, Emsley P, Evans PR, Keegan RM, Krissinel EB, Leslie AGW, McCoy A, McNicholas SJ, Murshudov GN, Pannu NS, Potterton EA, Powell HR, Read RJ, Vagin A & Wilson KS (2011) Overview of the CCP4 suite and current developments. *Acta Crystallogr D Biol Crystallogr* 67, 235–242.

60. Stein N (2008) CHAINSAW: a program for mutating pdb files used as templates in molecular replacement. *J Appl Cryst* 41, 641–643.

61. Emsley P, Lohkamp B, Scott WG & Cowtan K (2010) Features and development of Coot. *Acta Crystallogr D Biol Crystallogr* 66, 486–501.

62. Murshudov GN, Skubák P, Lebedev AA, Pannu NS, Steiner RA, Nicholls RA, Winn MD, Long F & Vagin AA (2011) REFMAC5 for the refinement of macromolecular crystal structures. *Acta Crystallogr D Biol Crystallogr* 67, 355–367.

63. Chen VB, Arendall WB, Headd JJ, Keedy DA, Immormino RM, Kapral GJ, Murray LW, Richardson JS & Richardson DC (2010) MolProbity: all-atom structure validation for macromolecular crystallography. *Acta Crystallogr D Biol Crystallogr* 66, 12–21.

TABLES

Table 1. Lysine inhibition affinities (IC_{50}) of DHDPS enzymes from Gram-negative bacteria.

	IC_{50} (µM)
KpDHDPS	160
AbDHDPS	160
EcDHDPS[#]	180
PaDHDPS2*	130

As determined in [#][35] and *[23].

Table 2. Data collection and processing statistics for KpDHDPS.

Diffraction source	MX2, Australian Synchrotron
Wavelength (Å)	0.95374
Temperature (K)	100
Detector	EIGER-16M
Crystal-to-detector distance (mm)	150
Total rotation range (°)	180
Space group	$P2_12_12$
a, *b*, *c* (Å)	105.6, 114.2, 55.3
α, β, γ (°)	90, 90, 90
Mosaicity (°)	0.15
Resolution range (Å)	48.99-1.89 (1.93-1.89)
Total no. of reflections	362,343 (20,999)

No. of unique reflections	54,102 (3,259)
Completeness (%)	99.7 (95.3)
Multiplicity	6.7 (6.4)
$\langle I/\sigma(I)\rangle$	11.4 (1.9)
$CC_{1/2}$	0.998 (0.827)
R_{merge} (%)	8.0 (62.9)
R_{pim} (%)	5.0 (39.6)

Values in parentheses are for the highest resolution shell.

Table 3. Refinement statistics for KpDHDPS.

Resolution range (Å)	49.04-1.89 (1.94-1.89)
Completeness (%)	99.7 (96.3)
R (%)	17.0 (29.7)
R_{free} (%)	20.0 (31.7)
No. (%) of reflections in test set	3608 (4.7)
No. of protein molecules per asu	2
R.m.s.d. bond length (Å)	0.01
R.m.s.d. bond angle (°)	1.40
Average B-factors (Å^2)[a]	24.4
Protein molecules	23.7
Water molecules	31.3
Ramachandran plot[b]	

Residues other Gly and Pro in:	
Most favoured regions (%)	98.6
Additionally allowed regions (%)	1.4
PDB code entry	6UE0

Values in parentheses are for the highest resolution shell.

[a]Calculated by BAVERAGE in CCP4 Suite [59].

[b]Calculated using MolProbity [63].

FIGURE LEGENDS

Figure 1. Diaminopimelate pathway (DAP) in bacteria. The DAP pathway begins with the condensation of pyruvate and (*S*)-aspartate semialdehyde (ASA) by dihydrodipicolinate synthase (DHDPS) to produce 4-hydroxy-2,3,4,5-tetrahydro-(2*S*)-dipicolinic acid (HTPA). Dihydrodipicolinate reductase (DHDPR) then converts HTPA to 2,3,4,5-tetrahydrodipicolinate (THDP). At this point, the pathway branches into four sub-pathways; the acetylase (double line), dehydrogenase (dotted line), aminotransferase (dashed line) or succinyl pathway (solid line), which is commonly observed in Gram-negative bacteria. The sub-pathways all converge at the production of *meso*-DAP, which is irreversibly decarboxylated to lysine by diaminopimelate decarboxylase (DAP-DC).

Figure 2. Multiple sequence alignment of the putative *dapA* gene products from *Klebsiella pneumoniae* (KpDapA1 **UNIPROT ID: A6TCA1**, KpDapA2 **UNIPROT ID: A0A0H3GS49**, KpDapA3 **UNIPROT ID: B5Y2B8**, KpDapA4 **UNIPROT ID: W1DHJ6**) and *Acinetobacter baumannii* (AbDapA1 **UNIPROT ID: S3TLB4**, AbDapA2 **UNIPROT ID: A0A372I0L7**, AbDapA3 **UNIPROT ID: S3TI37**, AbDapA4 **UNIPROT ID: A0A022J7S0**), compared to *E. coli* DHDPS (**UNIPROT ID: P0A6L2**). Conservation of the active site residues required for catalysis are highlighted in black, with the DHDPS signature motif displayed above the alignment. Sequence alignment was performed using the ClustalW software embedded in BIOEDIT (v.7.2.0).

Figure 3. (A) SDS-PAGE summary showing the recombinant *K. pneumoniae dapA1-4* gene products (lanes 2-5, respectively) compared to the Broad Range Molecular Weight (10-200

kDa) ladder (Lane 1). **(B)** Circular dichroism (CD) spectra of recombinant KpDapA1 (blue), KpDapA2 (brown), KpDapA3 (teal) and KpDapA4 (red). The solid line represents the fit produced using the CONTINLL database and the SP22x reference set. **(C)** *o*-aminobenzaldehyde assay of KpDapA1-4 proteins, with *E. coli* DHDPS used as a positive control and *E. coli* DHDPR as a negative control.

Figure 4. (A) SDS-PAGE summary showing purified recombinant AbDapA1 compared to the Broad Range Molecular Weight (10-200 kDa) ladder, indicating a purity of >90%. **(B)** Circular dichroism (CD) spectrum of AbDapA1 with the fit produced using the CONTINLL database and the SP22x reference set (line). **(C)** *o*-aminobenzaldehyde assay of AbDapA1, with *E. coli* DHDPS and *E. coli* DHDPR as positive and negative controls, respectively.

Figure 5. (A-B) Kinetic profile of KpDHDPS plotted as initial velocity ($\mu mol \cdot min^{-1} \cdot mg^{-1}$) at varying concentrations of **(A)** pyruvate at 4.0 mM (○), 2.0 mM (□), 1.0 mM (△), 0.50 mM (◊) and 0.25 mM (▽) plotted as a function of ASA concentration and **(B)** ASA at 0.80 mM (●), 0.40 mM (■), 0.20 mM (▲), 0.10 mM (◆) and 0.05 mM (▼) plotted as a function of pyruvate concentration. **(C-D)** Kinetic profile of AbDHDPS plotted as initial velocity ($\mu mol \cdot min^{-1} \cdot mg^{-1}$) at varying concentrations of **(C)** pyruvate at 5.0 mM (○), 2.5 mM (□), 1.3 mM (△), 0.63 mM (◊), 0.32 (▽) and 0.078 mM (▯) plotted as a function of ASA concentration and **(D)** ASA at 0.50 mM (●), 0.25 mM (■), 0.13 mM (▲), 0.063 mM (◆), 0.032 (▼) and 0.0078 mM (▯) plotted as a function of pyruvate concentration. All data was fitted to a bi-substrate ping-pong model without substrate inhibition using ENZFITTER software (v.2.0.18), which resulted in an R^2 value of 0.98. Data are represented as mean ± standard deviation (n = 3).

Figure 6. (A) Overall structure of KpDHDPS in a head-to-head dimer of dimer arrangement (**PDB ID: 6UE0**). **(B)** Superposition of the active sites of pyruvate-bound EcDHDPS (orange) (**PDB ID: 3DU0**), pyruvate-bound AbDHDPS (pink) (**PDB ID: 3TAK**), pyruvate-bound KpDHDPS (blue) (**PDB ID: 6UE0**) and apo PaDHDPS2 (green) (**PDB ID: 3NOE**), highlighting the key residues involved in catalytic activity. **(C)** Superposition of EcDHDPS (orange) (**PDB ID: 3DU0**) and PaDapA4 (purple) (**PDB: 3NA8**) demonstrates the differences in the active site residues. Images were generated using PYMOL v.1.3 (Schrodinger, New York, NY, USA).

FIGURES

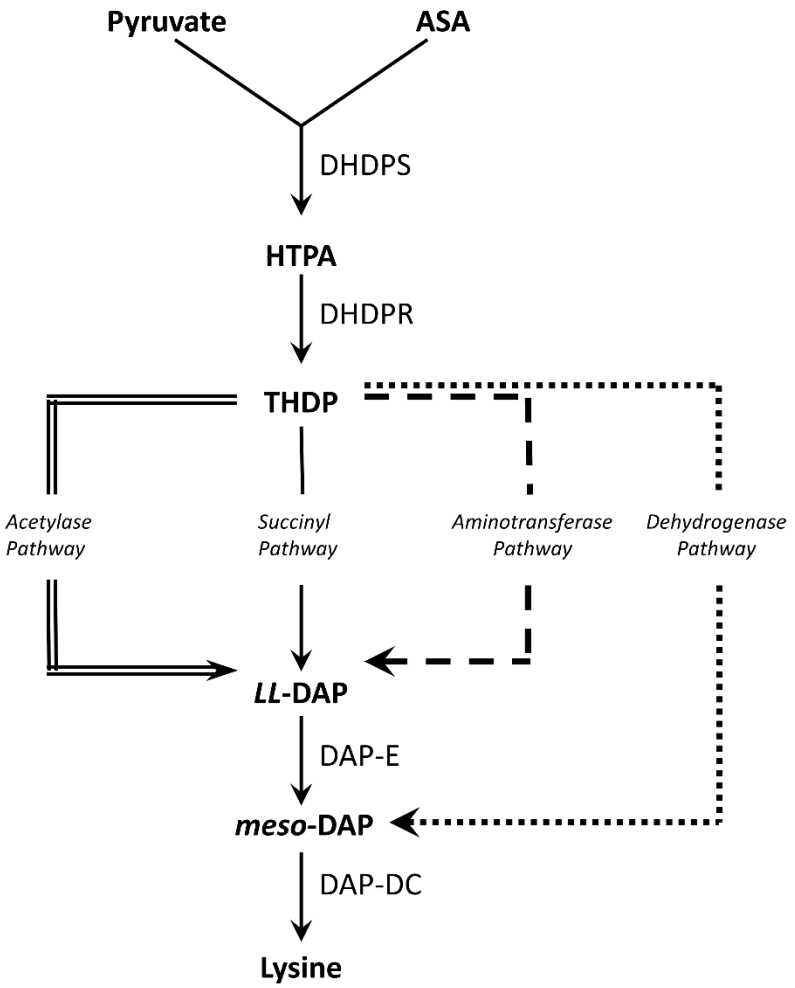

FIGURE 1

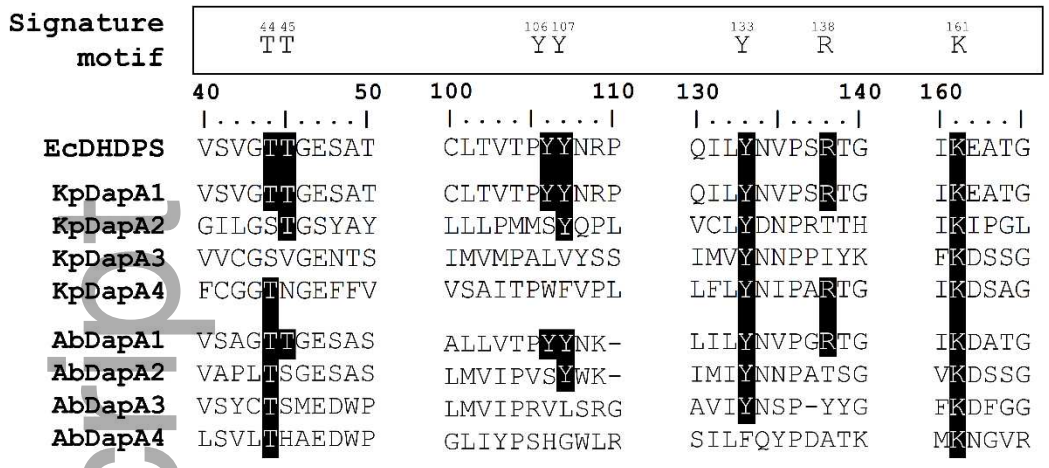

FIGURE 2

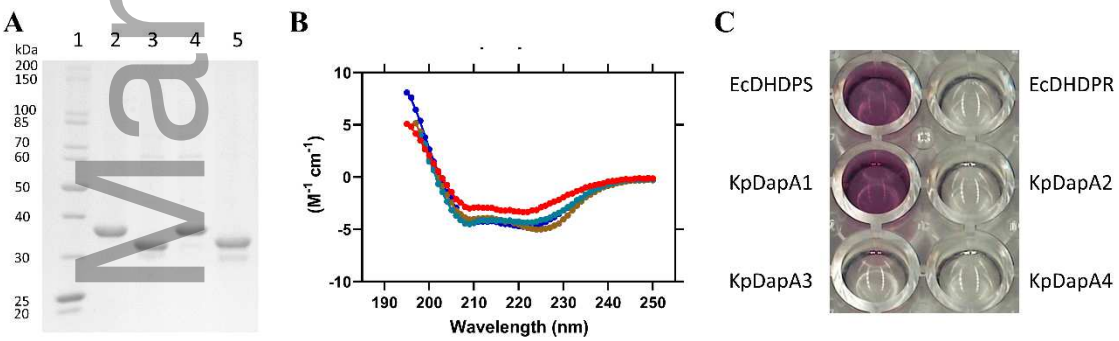

FIGURE 3

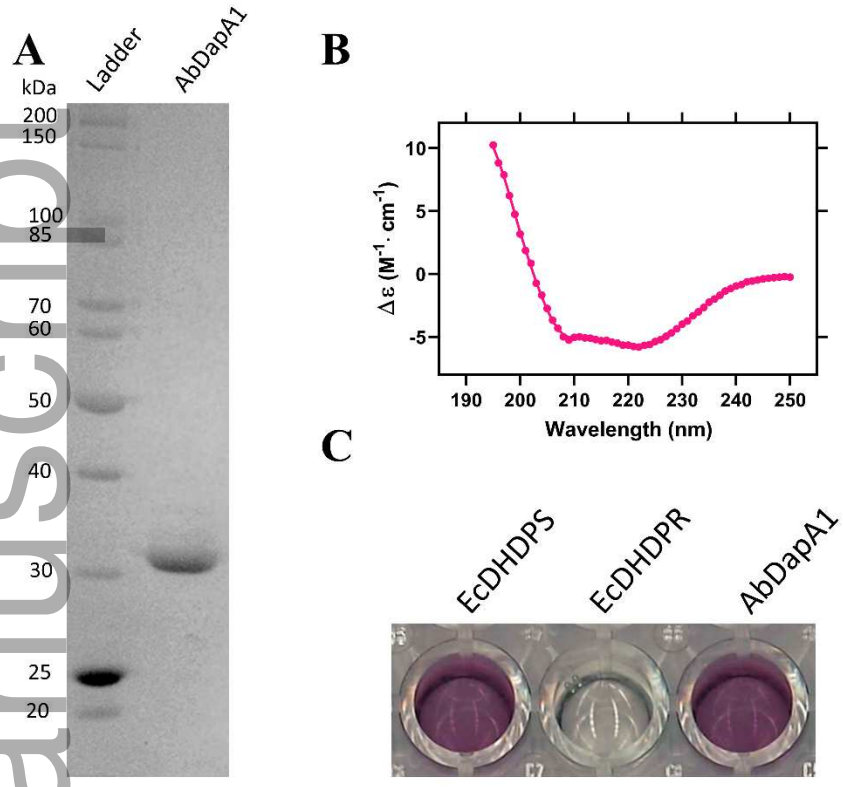

FIGURE 4

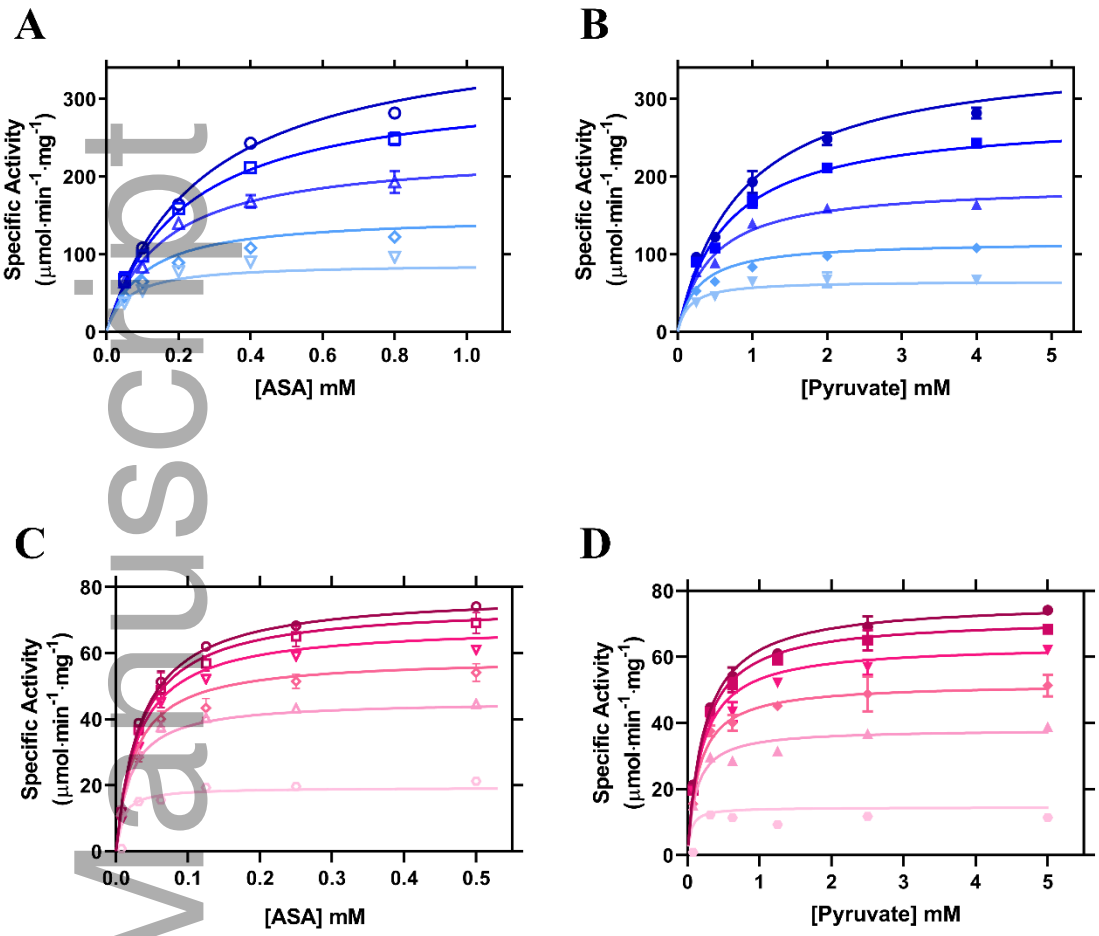

FIGURE 5

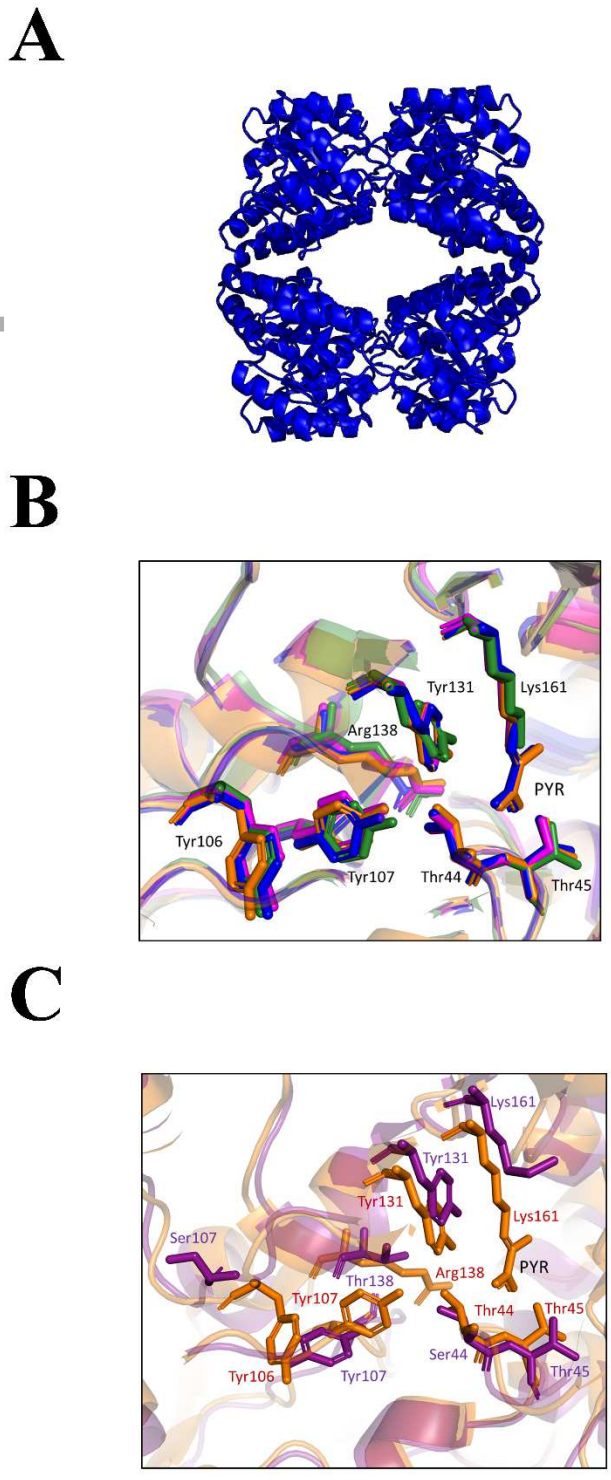

FIGURE 6

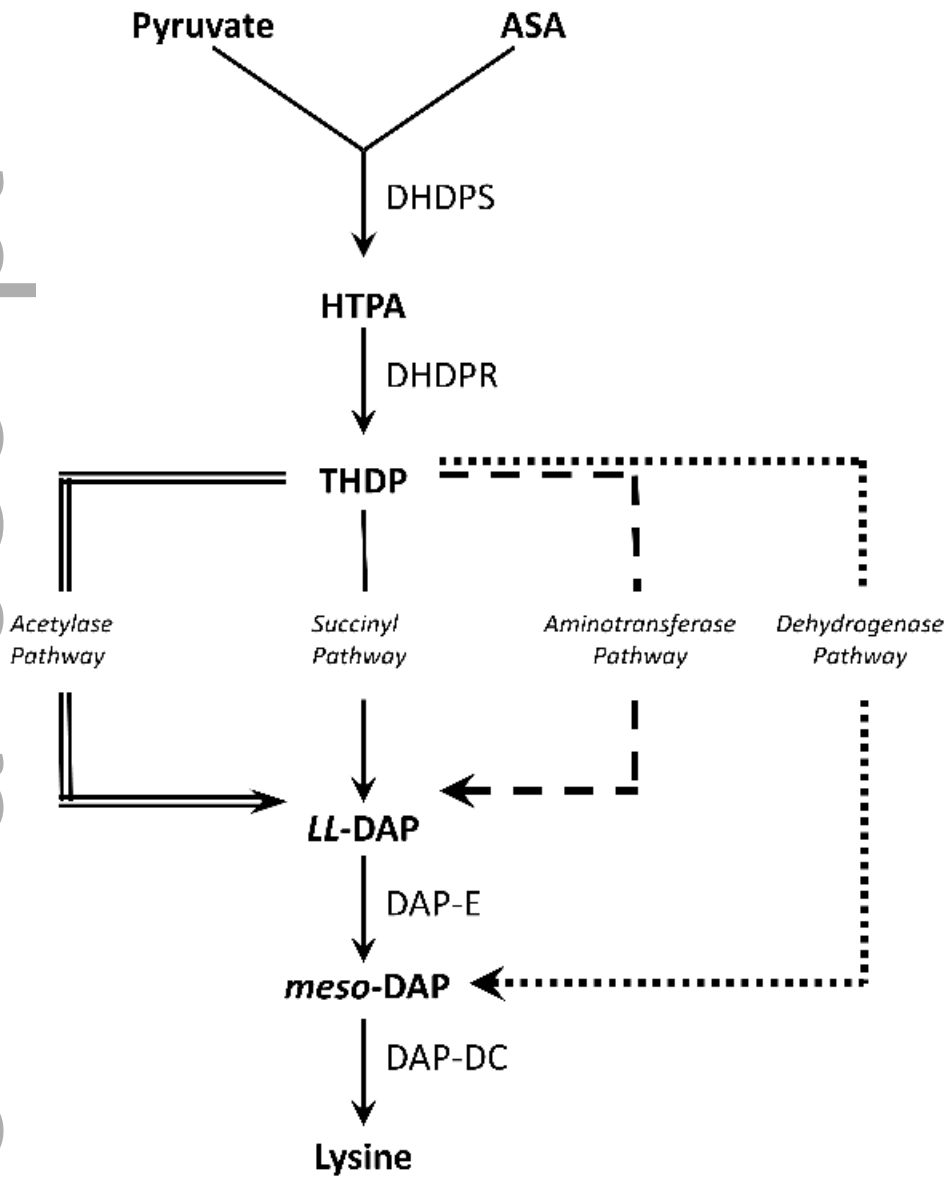

feb2_13733_f1.tif

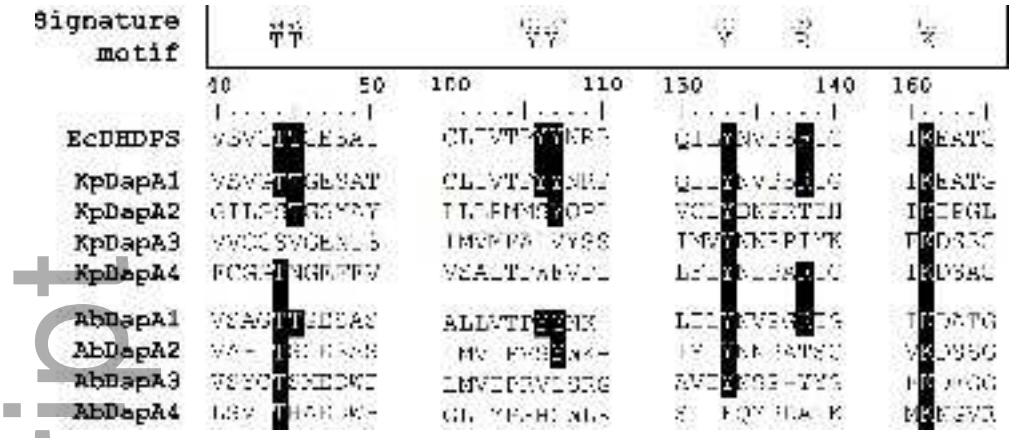

feb2_13733_f2.tif

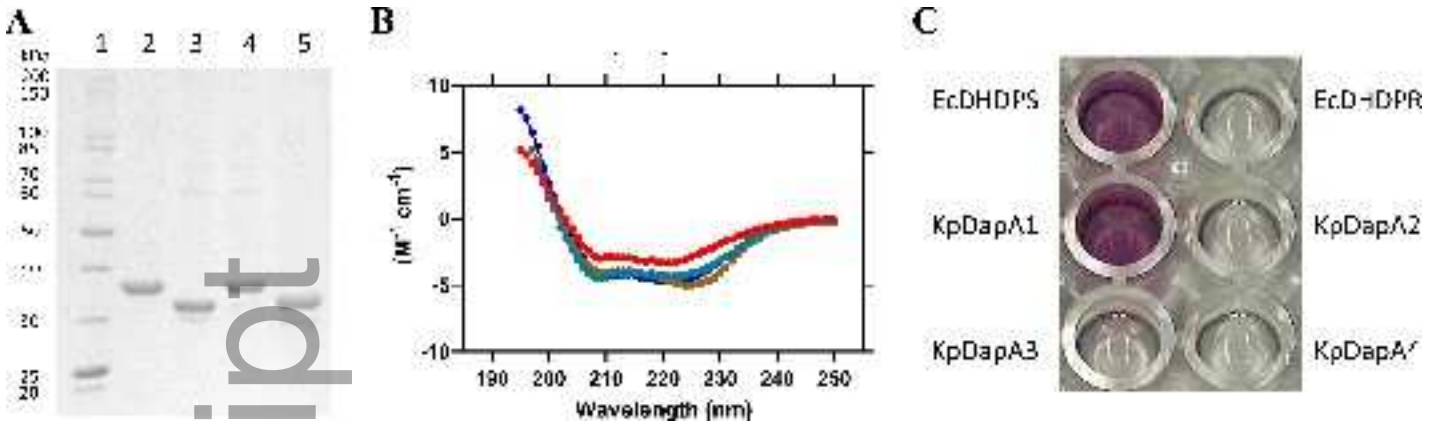

feb2_13733_f3.tif

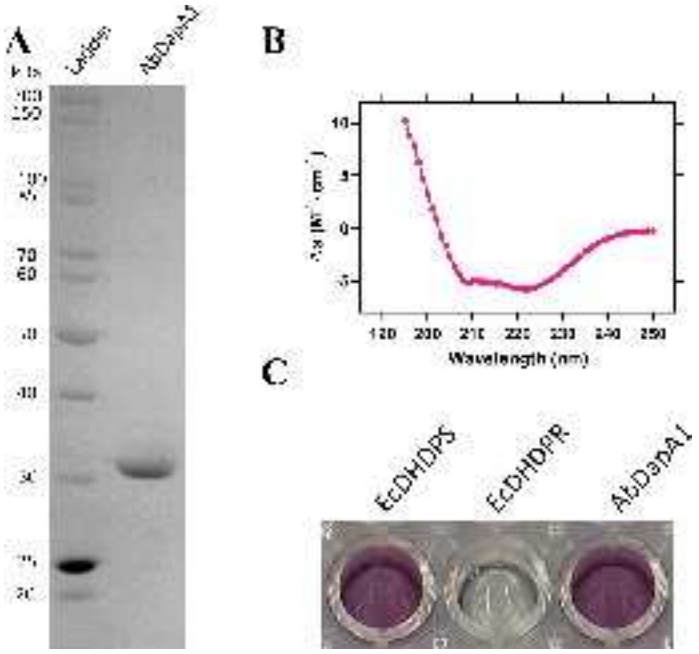

feb2_13733_f4.tif

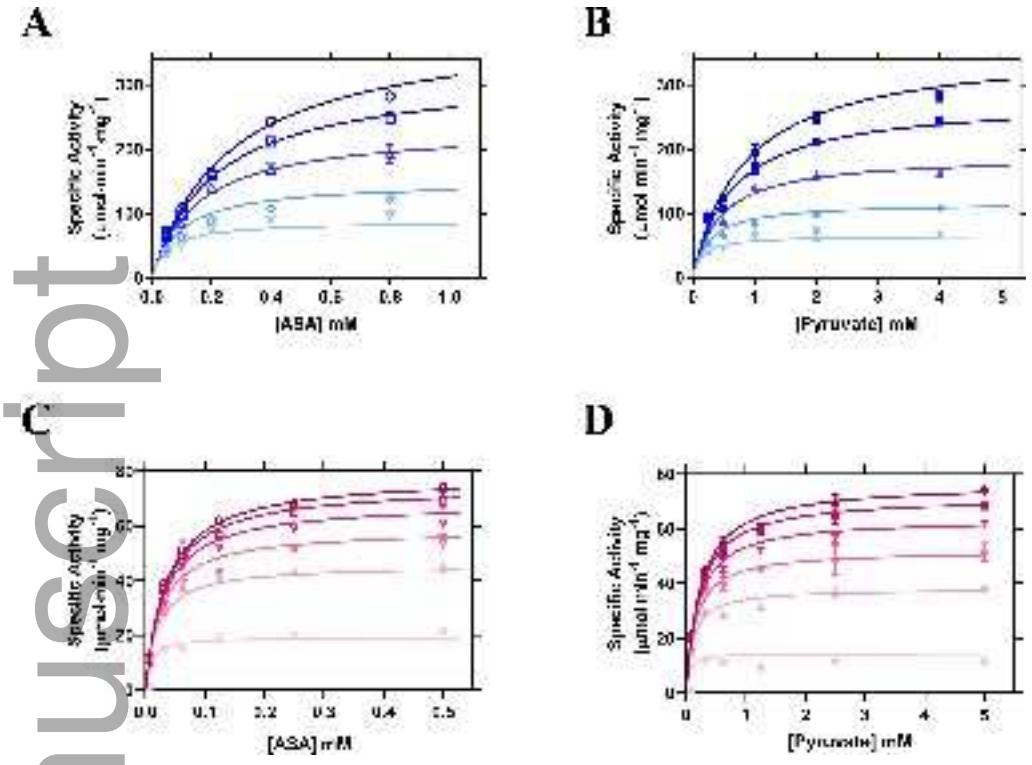

feb2_13733_f5.tif

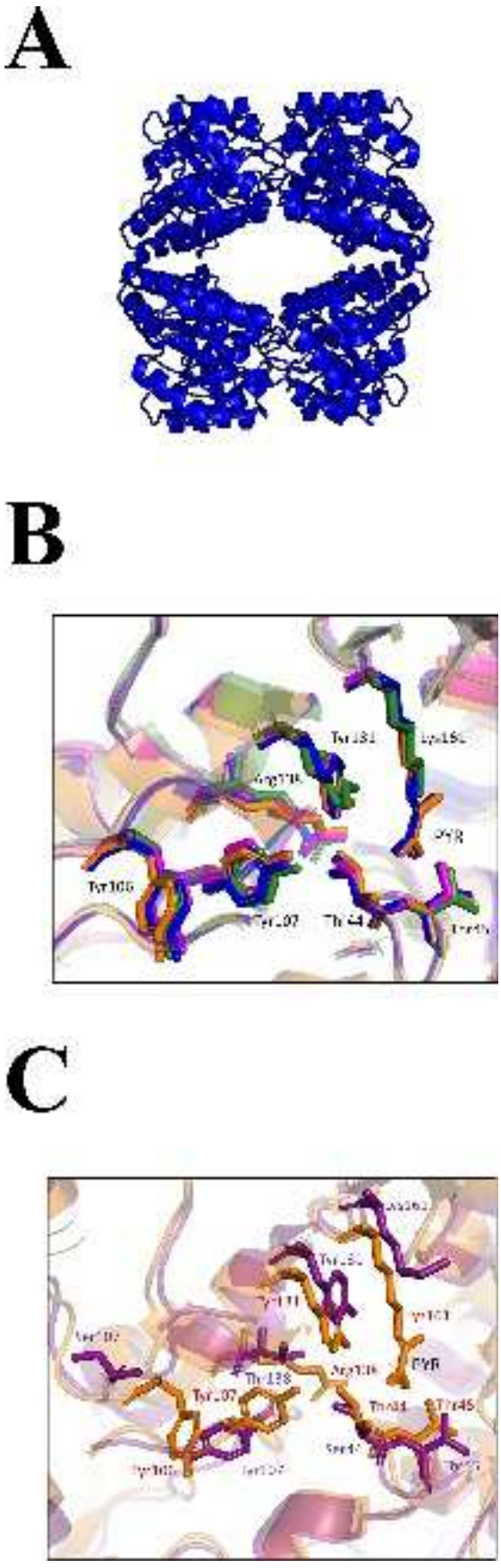

feb2_13733_f6.tif